NeuroImage 96 (2014) 133–142

Contents lists available at ScienceDirect

NeuroImage

journal homepage: www.elsevier.com/locate/ynimg

Neuronal transport defects of the MAP6 KO mouse – a model of schizophrenia – and alleviation by Epothilone D treatment, as observed using MEMRI

Alexia Daoust [a,b], Sylvain Bohic [a,b,c], Yasmina Saoudi [b,d,e], Clément Debacker [a,b,f], Sylvie Gory-Fauré [b,d,e], Annie Andrieux [b,d,e], Emmanuel Luc Barbier [a,b,*,1], Jean-Christophe Deloulme [b,d,e,*,1]

[a] Inserm U836, Equipe NeuroImagerie Fonctionnelle et Perfusion Cérébrale, BP170, Grenoble 38042, France
[b] Université Joseph Fourier, Grenoble Institut des Neurosciences, Grenoble, France
[c] European Synchrotron Radiation Facility (ESRF), Grenoble, France
[d] Inserm U836, Equipe Physiopathologie du Cytosquelette, Grenoble, France
[e] Commissariat à l'Energie Atomique et aux Energies Alternatives, iRTSV-GPC, Grenoble, France
[f] Bruker Biospin MRI, Ettlingen, Germany

ARTICLE INFO

Article history:
Accepted 25 March 2014
Available online 3 April 2014

Keywords:
MAP6
Manganese
MEMRI
Neuronal tract
Epothilone D

ABSTRACT

The MAP6 (microtubule-associated protein 6) KO mouse is a microtubule-deficient model of schizophrenia that exhibits severe behavioral disorders that are associated with synaptic plasticity anomalies. These defects are alleviated not only by neuroleptics, which are the gold standard molecules for the treatment of schizophrenia, but also by Epothilone D (Epo D), which is a microtubule-stabilizing molecule. To compare the neuronal transport between MAP6 KO and wild-type mice and to measure the effect of Epo D treatment on neuronal transport in KO mice, $MnCl_2$ was injected in the primary somatosensory cortex. Then, using manganese-enhanced magnetic resonance imaging (MEMRI), we followed the propagation of Mn^{2+} through axonal tracts and brain regions that are connected to the somatosensory cortex. In MAP6 KO mice, the measure of the MRI relative signal intensity over 24 h revealed that the Mn^{2+} transport rate was affected with a stronger effect on long-range and polysynaptic connections than in short-range and monosynaptic tracts. The chronic treatment of MAP6 KO mice with Epo D strongly increased Mn^{2+} propagation within both mono- and polysynaptic connections. Our results clearly indicate an *in vivo* deficit in neuronal Mn^{2+} transport in KO MAP6 mice, which might be due to both axonal transport defects and synaptic transmission impairments. Epo D treatment alleviated the axonal transport defects, and this improvement most likely contributes to the positive effect of Epo D on behavioral defects in KO MAP6 mice.

Introduction

The neurobiology of psychiatric disorders remains unclear; however, there is increasing evidence of white matter abnormalities (Fitzsimmons et al., 2009; Palau-Baduell et al., 2012) together with regional volumetric defects that are associated with a reduction in tract size and with abnormal microstructures. Furthermore, anomalies in neuronal transport that were initially reported in neurodegenerative diseases, including Alzheimer's disease, Huntington's disease and amyotrophic lateral sclerosis (ALS) (De Vos et al., 2007; Stokin et al., 2005; Szebenyi et al., 2003), are now strongly suggested in psychiatric disorders (Costas et al., 2013; Friocourt et al., 2011; Taya et al., 2007; Willemsen et al., 2012). *In vitro*, axonal transport is usually directly measured using cultured neurons to analyze cargo traffic. *In vivo*, neuronal transport integrates not only axonal transport but also synaptic transmission and tools to characterize neuronal transport in live animals and the effect of a pharmacological treatment on transport parameters are of great interest. In this respect, manganese-enhanced magnetic resonance imaging (MEMRI) (Bertrand et al., 2013; Smith et al., 2007), which relies on the use of manganese (Mn^{2+}) as a contrast agent, is an extremely powerful technique for characterizing neuronal transport in animals. Similar to gadolinium, Mn^{2+} decreases T_1 and T_2 relaxation times. Mn^{2+} is able to enter neurons through voltage-dependent calcium (Ca^{2+}) channels (Narita et al., 1990), is transported along axons and can cross synapses (Pautler, 2004; Pautler and Koretsky, 2002; Pautler et al., 1998; Saleem et al., 2002). Thus, when locally injected, Mn^{2+} acts as an anterograde trans-synaptic tracer that allows the track-tracing kinetic of specific neuronal tracts. This method has been used to analyze several neuronal pathways, including

Abbreviations: MAP, microtubule-associated protein; MEMRI, manganese-enhanced magnetic resonance imaging; KO, knockout.

* Corresponding authors at: Inserm U836, BP 170, Site Santé La Tronche, 38042 Grenoble Cedex 9, France.
E-mail addresses: emmanuel.barbier@ujf-grenoble.fr (E.L. Barbier), jean-christophe.deloulme@ujf-grenoble.fr (J.-C. Deloulme).

[1] These authors equally shared the supervision of this study.

http://dx.doi.org/10.1016/j.neuroimage.2014.03.071

noradrenergic, corticocortical or corticothalamic tracts (Bearer et al., 2009; Pautler and Koretsky, 2002; Pautler et al., 1998; Soria et al., 2008; Tucciarone et al., 2009; Van der Linden et al., 2002; Yu et al., 2005).

In this study, we evaluate *in vivo* neuronal transport in the MAP6/STOP KO mouse, which is an animal model of a psychiatric disorder where the microtubule-associated protein MAP6 has been deleted (Andrieux et al., 2002). MAP6 KO mice exhibited neuroanatomical deficits, such as a reduction in brain volume (Powell et al., 2007), which is associated with behavioral disorders that are associated with several alterations in many neurotransmission systems (Andrieux et al., 2002; Bouvrais-Veret et al., 2007; Brenner et al., 2007; Brun et al., 2005; Fournet et al., 2010). These behavioral and neurochemical alterations, which recapitulate some of the clinical features of schizophrenia, have been shown to be alleviated by chronic treatment with typical or atypical antipsychotics (Bégou et al., 2008; Delotterie et al., 2010). Interestingly, microtubule-related drugs, such as Epo D (KOS-862) or NAP (davunetide), ameliorated the cognitive behavior of MAP6 deficient mice (Andrieux et al., 2006; Fournet et al., 2012; Merenlender-Wagner et al., 2010), which indicated that the pharmacological modulation of microtubule dynamics/stability might regulate integrated brain functions. Moreover, synaptic deficits in the brains of the MAP6 KO mice, corresponding to a decrease of synaptic vesicle pools and the impairment of synaptic plasticity, have been shown (Andrieux et al., 2002). We hypothesized that MAP6 KO mice might present a reduction in neuronal transport that would be detectable by MEMRI.

Here, using MEMRI, we assayed neuronal transport within somatosensory cortex projections of MAP6 KO mice compared with wild-type animals. We found that MAP6 KO mice exhibited an altered neuronal transport capacity, which was associated with the alteration of some white matter tracts. Interestingly, we showed that Epo D treatment was able to alleviate the neuronal transport defects that were exhibited by MAP6 KO mice.

Materials and methods

Mice and experiments

All experiments were performed on a C57Bl6/129SvPas-F1 genetic background. The homogeneous inbred C57BL6/129SvPas-F1 mice were obtained by crossing pure heterozygote 129SvPas MAP6 mice with pure heterozygote C57BL6 MAP6 mice. All experiments were conducted on female wild type (WT) (n = 10) and MAP6 KO (n = 30) littermate mice at 3–6 months of age, in compliance with the European Community Council Directive of November 24, 1986 (86/609/EEC) (permit number 81105 for A.D.; agreement of ethics committee n°004).

Two different experiments that were performed in this study are summarized below.

In experiment 1 (related to Figs. 1, 2 and 3), Mn^{2+} transport was assessed *in vivo* using MEMRI in WT mice (n = 10) and in MAP6 KO mice (n = 10), and then, the mice were killed. Postmortem, the somatosensory cortex pathway was traced using the monosynaptic tracer DiI (n = 3 WT; n = 3 KO). Myelin tracts were labeled with gold chloride (n = 5 WT; n = 5 KO). In experiment 2 (related to Fig. 4), KO MAP6 mice were treated with Epo D (n = 10) or with the vehicle solution (n = 10). In both groups, Mn^{2+} transport was assessed using MEMRI before and after treatment.

MEMRI

Surgery and tracer injection

Hydrated manganese chloride (100 mM, $MnCl_2$–$4H_2O$, M1787, Sigma-Aldrich, St Louis, MO, USA) was dissolved in 10 mM Tris–HCl, pH 7.3. The Mn^{2+} solution was filtered through 0.2 μm membranes before use. For Mn^{2+} administration, animals were sedated with an intraperitoneal (ip) injection of xylazine (10 μL/g; 0.1% diluted in NaCl 9/1000; Rompun®, Virbac, France). Five minutes later, anesthesia was induced by an ip injection of ketamine (10 μL/g; 10 g/L diluted in NaCl 9/1000; Imalgène 1000®, Virbac, France). Animals were placed in a stereotaxic frame. The coordinates were determined following the Paxinos and Franklin atlas (Paxinos and Watson, 1998). A hole was drilled in the skull, and through this hole, a 34 G silica cannula (Phymep, France) was implanted into the primary somatosensory cortex (S1) (anterior–posterior: −0.6 mm; lateral: −2.0 mm; and ventral: −0.7 mm). Sixty nanoliters of Mn^{2+} solution were instilled at a rate of 8 nL/min *via* a connected Hamilton syringe. Ten minutes after the end of the injection, the cannula was retracted stepwise to avoid leakage of the tracer along the injection track. After surgery, the skin was sutured, and animals received a local anesthetic (bupivacaine, Vétoquinol, France) directly on the wound. Animals also received a subcutaneous injection of an anti-inflammatory (caprofen; 5 μg/g, Rimadyl®, Virbac, France) and antibiotics (sulfadoxine 20% and trimethoprim 4%; 0.125 μL/g, Borgal®, Virbac, France). Throughout the entire surgical procedure, the rectal temperature was maintained at 37 °C with a heating pad.

In vivo MRI

MRI was performed 2, 6, 10 and 24 h after $MnCl_2$ injection in a horizontal 7T MRI system (Avance III, Bruker, Ettlingen, Germany) using a surface/volume cross coil configuration. Anesthetized animals (isoflurane (IsoFlo, Axience, France); 5% for induction, maintenance under 2.5%) were placed in a dedicated cradle, which was equipped with bite and ear bars. T_1-weighted images were obtained (MDEFT 3D, TR/TE = 4000/3.65 ms, TI = 1000 ms, voxel size: 109 × 109 × 250 μm). The acquisition duration was 17 min. The temperature and the breathing rate were monitored.

The MRI data were analyzed using software that was developed in the Matlab environment (Mathworks, Natick, MA, USA). Five regions of interest (ROI) were manually drawn in ipsi- and contralateral hemispheres: internal capsule (ic), somatosensory cortex S1 (S1), anterior (Ant. TH) and posterior (Post. TH) thalamus and the cerebral peduncle (cp). The signal from the ipsilateral S1 ROI, which corresponded to the injection site, was used as a reference to compensate for the variability in the injected amount of Mn^{2+} solution. Therefore, the MEMRI signal that was measured in each ROI was divided by the MEMRI signal that was measured in the ipsilateral S1 ROI. The normalized MEMRI signal is called the relative signal intensity (RSI) for the rest of the manuscript.

Histology

After the ip administration of a lethal dose of sodium pentobarbital (100 mg/kg; Dolethal, IPV, France), all experiment 1 animals were transcardially perfused with a 4% PFA solution as described previously (Raponi et al., 2007). The brains were removed from the skulls, stored overnight in a 4% PFA solution at 4 °C and distributed into two groups for two different histological procedures.

Cortical tract tracing

A DiI crystal (1,1′-dioctadecyl-3,3,3′,3′-tetramethyl-indocarbocyanine perchlorate, Sigma) was placed in the injection site that was used for the Mn^{2+} solution. DiI is a lipid diffusing along axons throughout the plasma membrane, from the cell body to the synapse. It does not cross synapses. After three months of incubation at 37 °C in 4% PFA solution, coronal (n = 2 WT; n = 2 KO) and sagittal (n = 1 WT; n = 1 KO) sections (30 μm thick) were obtained using a vibrating blade microtome (VT1000S, Leica Biosystem, Nanterre, France). Sections were placed on glass slides, and coverslips were mounted using fluorescent mounting medium (Scytek, Logan, UT, USA). Each section was digitized using a DMI6000 microscope (Leica Biosystem, Nanterre, France), which was equipped with a 40× dry objective and an EMCCD Quantum camera that was driven by the Metamorph software (Roper Scientific, Every, France).

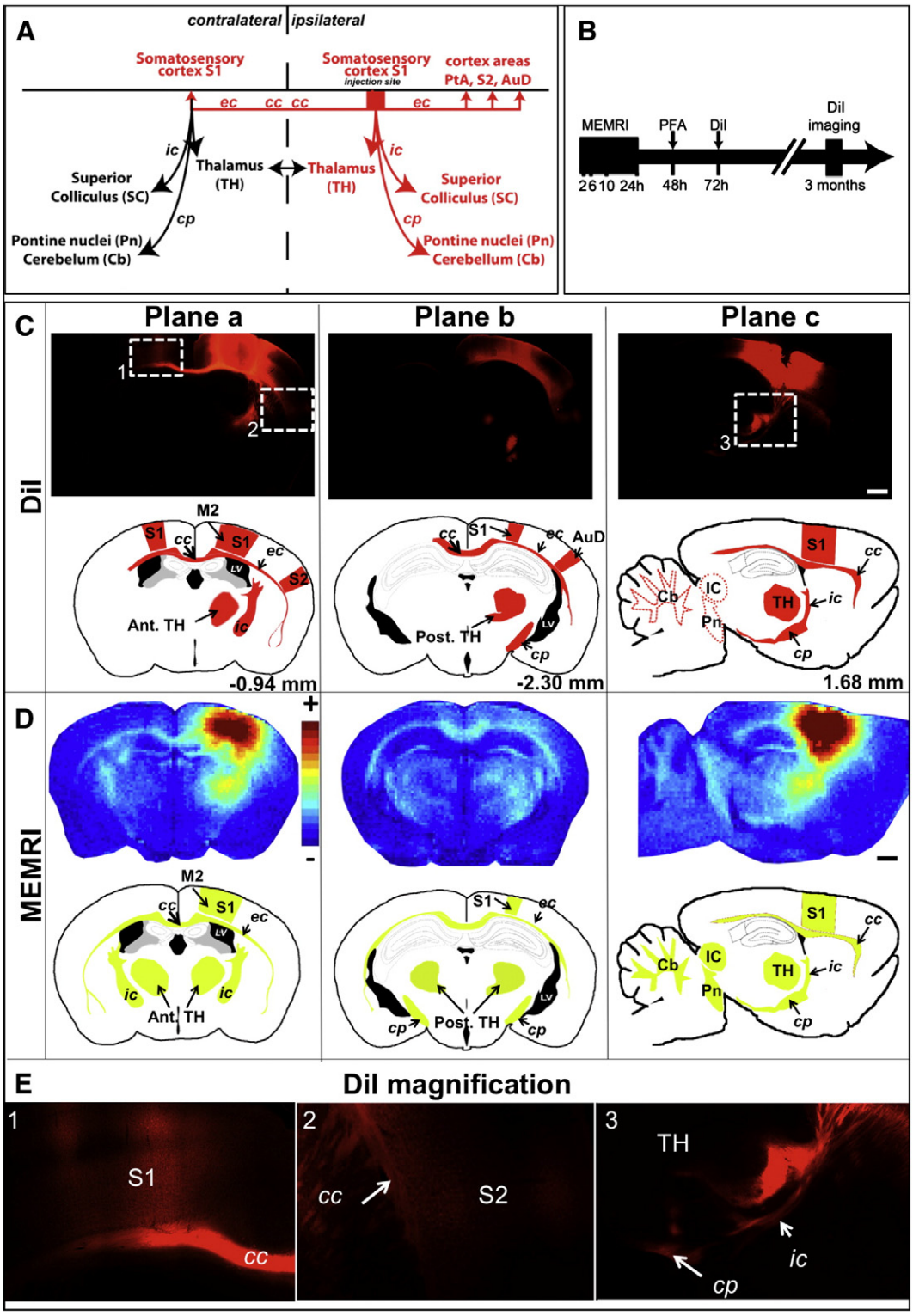

Fig. 1. Mono- and polysynaptic pathways of the somatosensory cortex, as revealed by DiI implantation and by MEMRI. (A) Schematic representation of major brain regions mono- (red) and polysynaptically (black) connected to the ipsilateral somatosensory cortex S1 (injection site). (B) Chronogram of the experiments, related to this figure and to Fig. 2 (detailed in the Materials and methods section). The MEMRI technique is composed of an intracerebral injection of Mn^{2+} into the cortex S1, following by four MRI acquisitions at 2, 6, 10 and 24 h after Mn^{2+} injection. Following MEMRI, mice were fixed with PFA, and DiI crystals were implanted in the same injection site as Mn^{2+}. DiI fluorescence signal was assayed after an incubation period of three months in PFA fixative solution. (C–D) DiI (C) and MEMRI (D) images (10 h) that correspond to the same brain of one WT mouse. Three anatomic planes are represented: anterior coronal (plane a), posterior coronal (plane b) and sagittal (plane c). For each technique, the imaging is shown (top), and the corresponding signal is diagrammed on an anatomical plane (bottom). (E) High magnification of squared areas that are shown in DiI panels in C. Scale bar: 1 mm. In coronal planes (a and b) and in the sagittal plane c, bregma and lateral are respectively indicated in mm. Abbreviations: Ant. TH: anterior thalamus; Cb: cerebellum; cc: corpus callosum; cp: cerebral peduncle; ic: internal capsule; IC: inferior colliculus; Pn: Pontine nuclei; S1: primary somatosensory cortex; S2: secondary somatosensory cortex; Post. TH: posterior thalamus, LV: lateral ventricle, M: motor cortex and ec: external capsule.

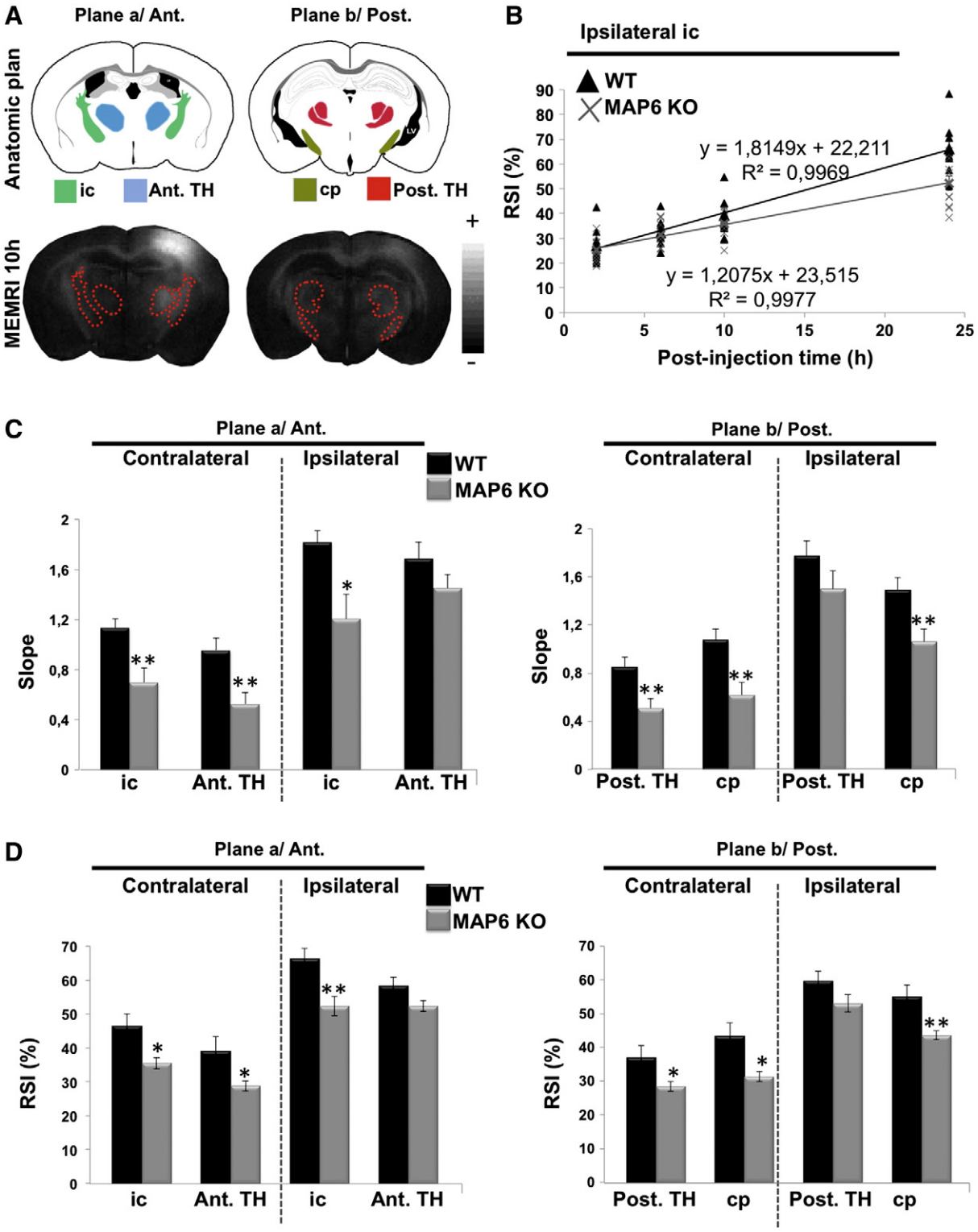

Fig. 2. MEMRI revealed a deficit of neuronal transport in MAP6 KO mice. (A) MEMRI acquisitions were performed at 2, 6, 10 and 24 h post-Mn^{2+} injection. All regions of interest (ROIs) were manually drawn on MEMRI images using their matched anatomic atlas plane as a reference. Diagrams represent matched anatomical planes with colored ROIs: internal capsule (ic, green); anterior thalamus (Ant. TH, blue); cerebral peduncle (cp, khaki) and posterior thalamus (Post. TH, red). Two representative MEMRI images of a WT brain at 10 h post-Mn^{2+} injection with ROIs (dotted red lines) were shown. Scale bar of MEMRI signal intensity is represented. (B) Representative graph of the relative signal intensity (RSI) evolution according to time after the Mn^{2+} injection in the ipsilateral internal capsule of WT and KO mice. RSI values increased linearly over the time and were significantly reduced in MAP6 KO mice. (C) Histograms of slope averages for ipsi- and contralateral ROIs. (D) Histograms of RSI averages for ipsi- and contralateral ROIs at 24 h after Mn^{2+} injection. n = 10 WT; n = 10 MAP6 KO. The values are the mean ± SEM. *p < 0.05; **p < 0.01. Abbreviations: Ant. TH: anterior thalamus; cp: cerebral peduncle; ic: internal capsule; Post. TH: posterior thalamus.

Myelin fiber characterization

Brains were placed in ascending concentrations of sucrose (10, 20 and 30% in PBS) until they sank, frozen in −40 °C isopentane and stored at −80 °C. Floating coronal sections (25 μm thick) were obtained around the injection site (+/−3 mm) using a cryomicrotome (Microm H 560, Microm Microtech, France). The sections were then stained using

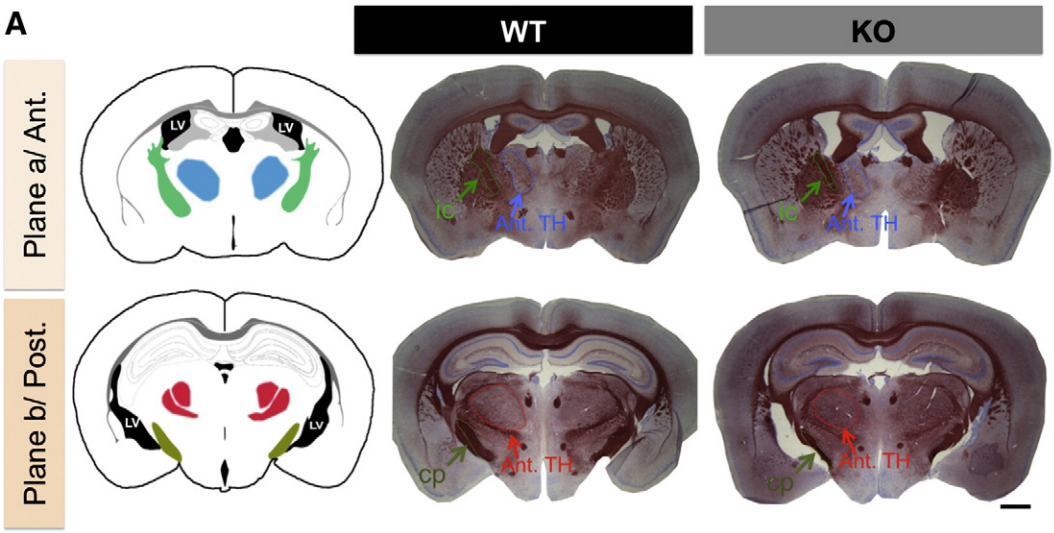

B

	plane a/ Ant.				plane b/ Post.			
	WT		KO		WT		KO	
Area mm²	contra.	ipsi.	contra.	ipsi.	contra.	ipsi.	contra.	ipsi.
cp					0.57±0.06	0.60±0.05	0.42±0.02*	0.44±0.01*
ic	0.94±0.13	0.90±0.05	0.50±0.04*	0.44±0.05***				
TH	1.08±0.06	1.08±0.08	0.77±0.03**	0.77±0.03**	2.59±0.26	2.59±0.12	1.95±0.06*	1.86±0.06***

Fig. 3. The internal capsule and the cerebral peduncle were reduced in MAP6 KO mice. (A) Representative brain sections in anterior and posterior planes are shown with their matched coronal diagrams. After chloride gold and cresyl violet staining, the myelinated fiber tracts appeared in red, and cellular bodies appeared in blue. Note the size reduction of the internal capsule (ic, green arrows) and of the cerebellar peduncle (cp, khaki arrows) in MAP6 KO mice. The reduction in these tracts was associated with a reduction in projection areas, such as the thalamus (Ant. TH, blue arrows and Post. TH, red arrows). ROIs are indicated with dotted colored lines. (B) Table showing surface areas of brain regions and comparisons of areas between WT and KO mice. n = 5 WT; n = 5 KO MAP6. The values are the mean ± SEM (*p < 0.05; **p < 0.01; ***p < 0.001). Scale bar = 1 mm. Abbreviations: cp: cerebral peduncle; cc: corpus callosum; ic: internal capsule; Ant. TH: anterior thalamus; Post. TH: posterior thalamus.

the gold chloride method of Schmued (Schmued et al., 2008). Briefly, sections were rinsed three times in PBS and incubated with 0.2% gold chloride for 2 h at room temperature. To stop the reaction, sections were incubated in 2.5% sodium thiosulfate, which was diluted in distilled water, for 5 min. After three rinses in PBS, floating sections were mounted on Superfrost Plus slides (Menzel-Gläser), and neurons were counterstained with cresyl violet. Each section was digitized (stereo microscope EZ4 HD, Leica Biosystem, Nanterre, France) and analyzed using the ImageJ software. Four ROIs were drawn manually on each hemisphere (in Ant. and Post. sections) using a mouse brain atlas (Paxinos and Watson, 1998) as a reference (internal capsule, cerebral peduncle and anterior and posterior thalamus), and their area was determined.

Evaluation of the effect of Epo D

Epo D was provided by the Gesellschaft für Biotechnologische Forschung (GBF) (Braunschweig, Germany). Epo D chronic treatment was performed as previously described (Andrieux et al., 2006; Fournet et al., 2012). Briefly, one week after MEMRI was performed at 24 h post-injection, mice received an intraperitoneal injection (ip) of either 1 mg/kg Epo D (200 μL/30 g body weight; n = 10) or vehicle only, once a week for eight weeks. The drug was diluted in warm water from a 50 mg/mL stock solution in dimethyl sulfoxide (DMSO). In control animals, vehicle injections consisted of 200 μL of corresponding mixtures of DMSO alone in warm water. During the week following the last ip administration, mice underwent a second MEMRI session, which was performed 2, 6, 10 and 24 h after $MnCl_2$ injection.

Statistical analysis

The results were expressed as the mean ± S.E.M. Unpaired t-tests, which were performed using the Microsoft Excel software, were used to assess differences. Values were considered significant when $^{*}p < 0.05$, $^{**}p < 0.001$ and $^{***}p < 0.0001$. To evaluate whether the time after Mn^{2+} injection is a predictor of the RSI in MEMRI images, the p-value for Pearson's correlation coefficient (R^2) was computed.

Results

Tracing of the somatosensory pathway

Reduced sensory gating appears to be among the core features of schizophrenia (Patterson et al., 2008), and MAP6 KO mice exhibited abnormal prepulse inhibition (PPI), which is indicative of abnormal sensory-gating abilities (Fradley et al., 2005; Volle et al., 2013). Thus, we thought to examine the somatosensory neuronal circuit, which is a well-documented and characterized circuit (Leergaard et al., 2003; von Bartheld et al., 1990). The main efferent projections of the somatosensory cortex (S1 cortex) circuit are composed of corticocortical, corticopontine, corticothalamic and corticotectal projections throughout four major tracts: the corpus callosum (cc), the internal capsule (ic), the external capsule (ec) and the cerebral peduncle (cp) (Fig. 1A). We traced the somatosensory pathway by MEMRI and classical DiI tracing, which followed the time course that is illustrated in Fig. 1B. Because DiI is a lipophilic neuronal tracer that freely diffuses in the plasma membrane, DiI will allow the characterization of neuronal tracts and brain projection areas that are monosynaptically connected to the injection area. Three months after DiI implantation, the implantation site (somatosensory cortex 1, S1) and the neighboring motor cortex (M2) exhibited a strong fluorescence signal (Fig. 1C, plane a). As expected, DiI primarily diffused to ipsilateral structures, such as the internal capsule (ic), thalamic regions (Ant. TH, Post. TH), cerebral peduncle (cp) and cortical areas S2 (Fig. 1C, planes a–c and Fig. 1E). In the contralateral

side, only the S1 cortex, which was monosynaptically connected to the ipsilateral S1 cortex (Leergaard et al., 2003), was visible (Fig. 1C, plane a and Fig. 1E, panel 1). DiI appeared limited to short-range connections (5 to 10 mm); the monosynaptic connected brain stem regions, such as the superior colliculus (SC) and pontine nuclei (Pn), were totally devoid of fluorescence signal (Fig. 1C, plane c).

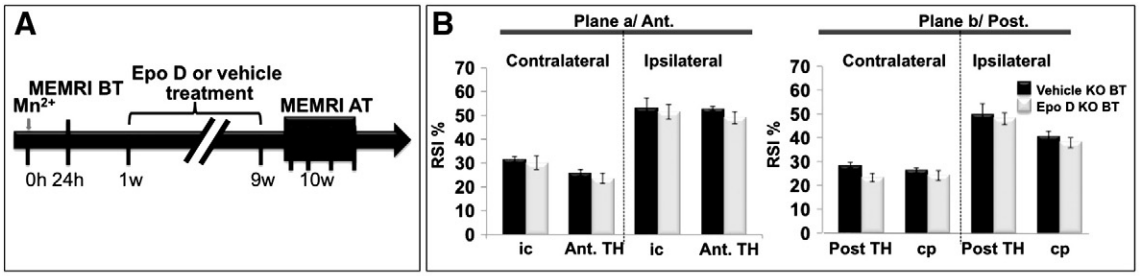

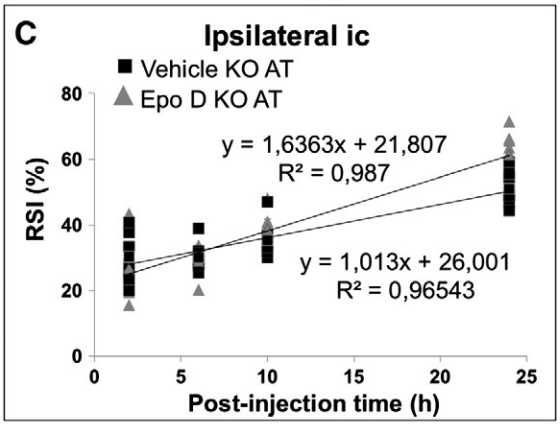

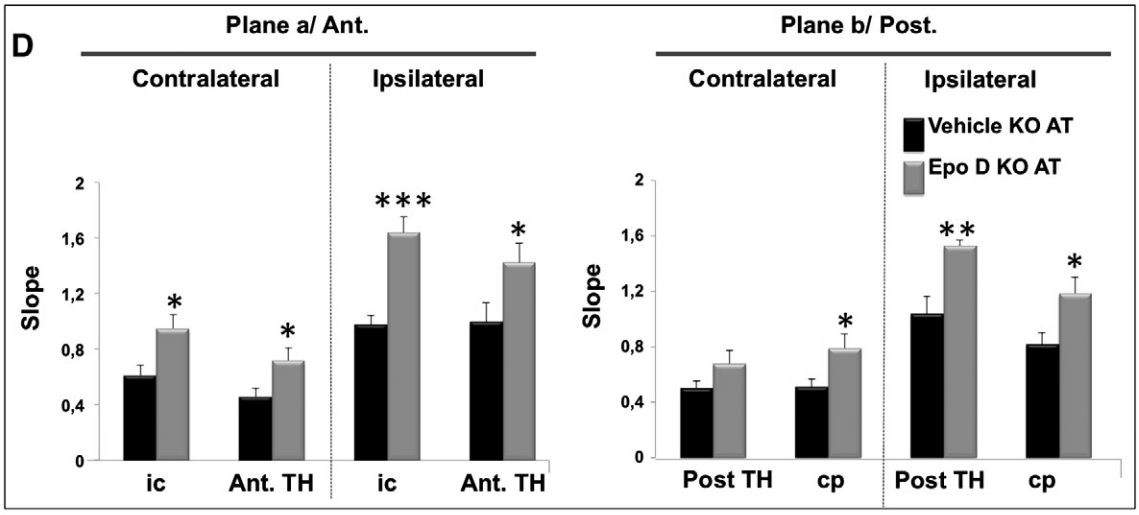

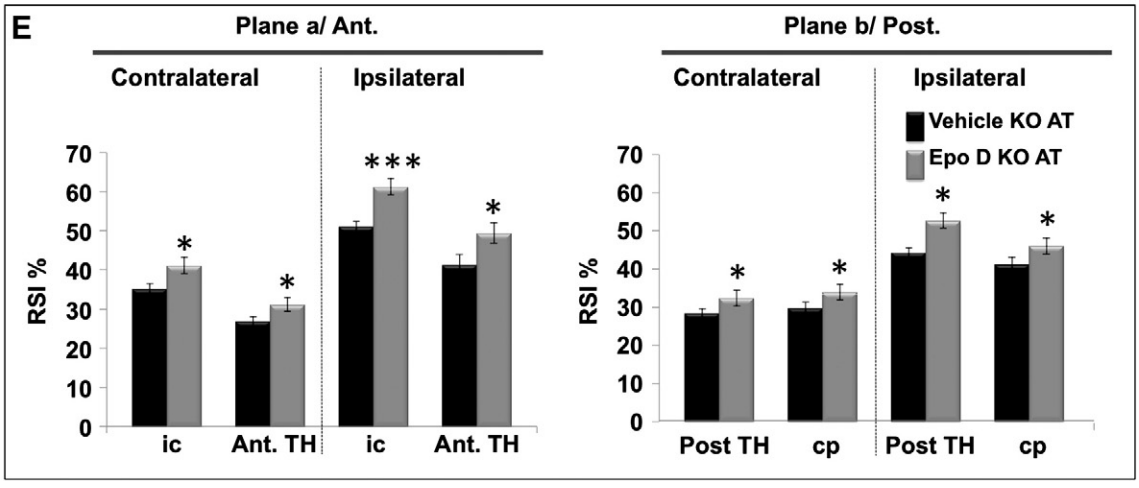

The somatosensory pathway tracing using MEMRI (Fig. 1D) revealed that Mn^{2+} transport was not restricted to monosynaptic and short-range connections. Two hours after Mn^{2+} injection, the MEMRI signal was hyperintense in the injection site (somatosensory cortex 1, S1) and in some structures of the ipsilateral hemisphere, but not in the hemisphere that was contralateral to the injection site (data not shown). Six and ten hours after Mn^{2+} injection (Fig. 1D), the MEMRI signal was extended to all ipsi- and contralateral structures that were associated with the somatosensory pathways, such as the anterior and posterior thalamus (Ant. TH, Post. TH), the corpus callosum (cc), the internal capsule (ic) and the cerebral peduncle (cp) (Fig. 1D, planes a–b). In the ipsilateral hemisphere, a slightly enhanced signal was also observed in the secondary somatosensory cortex (S2) and in the contralateral S1 cortex (data not shown). The sagittal view showed that the MEMRI signal was also enhanced in the brainstem, primarily in the inferior colliculus (IC), pontine nuclei (Pn) and the cerebellum (Cb) (Fig. 1D, plane c). Twenty-four hours after Mn^{2+} injection, the MEMRI signal was more diffuse than that observed at 10h; however, corticothalamic structures could still be readily depicted (data not shown).

However, in structures that were labeled by both Mn^{2+} and DiI, the MEMRI signal was more diffuse than that of DiI. This signal was particularly striking in the thalamus (Fig. 1C–D, planes a–b and Fig. 1E, panel 3).

Distribution patterns of Mn^{2+} or of DiI within the somatosensory structures of WT and MAP6 KO mice revealed no qualitative differences (data not shown), which suggested that all analyzed structures of the somatosensory pathway were properly connected in MAP6 KO mice.

Manganese neuronal transport in MAP6 KO mice

The neuronal transport capacity of wild-type and MAP6 KO mice was measured using MEMRI. Manganese relative signal intensities (RSI) between WT and KO MAP6 animals were measured (Fig. 2A) within equivalent tracts and brain regions that were monosynaptically (ipsilateral side) or polysynaptically (contralateral side) connected to S1 cortex injection site (Fig. 1A) at several time points (2, 6, 10 and 24 h). Within the ipsilateral internal capsule, RSI value increases linearly over time (ic; Fig. 2B and see Supplementary figure) in both WT ($R^2 = 0.9969$; $p = 1.6 \times 10^{-3}$) and KO MAP6 ($R^2 = 0.9977$; $p = 1.2 \times 10^{-3}$) mice; however, the comparison of slope values, which were relative to the speed of Mn^{2+} neuronal transport, was 33% lower in KO than in WT mice ($p = 0.011$). The linear increase of RSI over time was observed for all ipsi- and contralateral brain areas that were analyzed (data not shown). For all ipsi- and contralateral regions of interest (ROIs), we calculated slope values for WT and KO mice (histograms, Fig. 2C). In ipsilateral ROIs, slope values in MAP6 KO mice were 33% lower in the internal capsule and 29% lower in the cerebral peduncle than in WT (Fig. 2C, ic and cp, $p = 0.01$ and $p = 0.009$, respectively). Slope values in the anterior and posterior thalamus, although reduced in MAP6 KO mice, were not significantly different (Fig. 2C, Ant. TH and Post. TH, $p = 0.19$ and $p = 0.17$, respectively). In contralateral ROIs, all slope values from polysynaptic regions that were connected to S1 cortex were lower in KO MAP6 mice, with a reduction of 39% for the internal capsule (Fig. 2C, ic, $p = 0.006$), 45% for the anterior thalamus (Fig. 2C, Ant. TH, $p = 0.005$), 43% for the cerebral peduncle (Fig. 2C, cp, $p = 0.004$) and 41% for the posterior thalamus (Fig. 2C, Post. TH, $p = 0.009$). Statistical analysis showed that the neuronal transport rate of Mn^{2+} in KO mice had a more pronounced effect on contra- than on ipsilateral ROIs (−42% and −23%, respectively; $p = 0.024$).

RSI values, relative to the amount of accumulated manganese, that were measured 24 h after Mn^{2+} injection were reported in Fig. 2D. RSI values were lower in MAP6 KO mice and more affected in the contralateral side of KO mice. In ipsilateral ROIs, RSI values in MAP6 KO mice were lower by 21% in the internal capsule and by 21% in the cerebral peduncle (Fig. 2D, ic and cp, $p = 0.005$ and $p = 0.006$, respectively). RSI values in the anterior and posterior thalamus were not significantly different (Fig. 2D, Ant. TH and Post. TH, $p = 0.065$ and $p = 0.102$, respectively). In contralateral ROIs, all RSI values were reduced by 24% in the internal capsule (Fig. 2C, ic, $p = 0.012$), 26% in the anterior thalamus (Fig. 2D, Ant. TH, $p = 0.035$), 28% in the cerebral peduncle (Fig. 2D, cp, $p = 0.011$) and 23% in the posterior thalamus (Fig. 2D, Post. TH, $p = 0.049$). As observed for slope values, RSI reductions were more pronounced in contralateral than in ipsilateral ROIs (−21% and −15%, respectively; $p = 0.026$).

These MEMRI results showed that MAP6 KO mice exhibit neuronal transport deficits that affect both ipsi- and contralateral sides, with a more pronounced effect in the contralateral side that is possibly related to long-range and polysynaptic connections.

Axonal tract size in KO MAP6 mice

The neuronal transport deficit that was observed using MEMRI could involve a reduction in the size of axonal tracts. Thus, we performed gold staining of brain sections to assess the size of tracts and of some brain areas. After chloride gold and cresyl violet staining, the myelinated tracts appear in red, and cellular bodies appear in blue. The internal capsule (ic) and the cerebral peduncle (cp) appeared much smaller in KO MAP6 mice than in WT mice in both sides (Fig. 3A, ic and cp; arrows). In MAP6 KO mice, there are significant quantitative decreases for the internal capsule (Fig. 3B, ipsi. ic, −51%, $p = 1.6 \times 10^{-4}$; contra, −47%, $p = 0.013$) and for the cerebral peduncle (Fig. 3B, ipsi. cp, −27%, $p = 0.02$; contra. cp, −27%, $p = 0.01$). In MAP6 KO mice, the surfaces of the anterior and posterior thalamic structures were reduced in the same range as a previously reported reduction (Powell et al., 2007). In the MAP6 KO mouse brain, the anterior and the posterior thalamus were reduced (Fig. 3B, ipsi. Ant. TH, −29%, $p = 0.003$; Post. TH, −25%, $p = 0.04$; contra. Ant. TH, −28%, $p = 0.006$; Post. TH, −28%, $p = 0.006$).

This gold staining reveals that KO MAP6 exhibited strong and equal reductions in the size of internal capsule and of the cerebellar peduncle, which affected both hemispheres. Thus, if the reduction in axonal tract size can contribute to the abnormal neuronal transport in MAP6 KO, as detected using MEMRI, then other mechanisms, such as a reduction in the speed of axonal transport and/or abnormal synaptic transmission, are most likely present and may explain the more pronounced defects in the contra- compared with the ipsilateral side.

Effect of Epo D on neuronal transport in MAP6 KO mice

Epothilone D (Epo D) is a taxol-like microtubule stabilizing compound that has been previously shown to improve behavioral and synaptic deficits of MAP6 KO mice (Andrieux et al., 2006). Using MEMRI, we assayed whether a chronic treatment with Epo D might improve the neuronal transport deficit that has been observed in MAP6 KO mice (Fig. 4A). Before treatment (BT) with Epo D, manganese RSI values

Fig. 4. Epo D improved the neuronal transport of Mn^{2+} in KO MAP6 mice. (A) chronogram of the experiment. One week before Epo D or vehicle treatment (BT), MEMRI was performed on two groups of KO mice at 24 h after Mn^{2+} injection. One week after the MEMRI, Epo D or vehicle was weekly injected into KO MAP6 mice for eight weeks. One week after the end of the treatment (AT), Mn^{2+} neuronal transport was assessed by MEMRI sessions at 2, 6, 10 and 24 h post-Mn^{2+} injection. (B) Histograms of RSI values at 24 h after Mn^{2+} injection in MAP6 KO mice before treatment (Epo D or vehicle). (C) Representative graph of the relative signal intensity (RSI) evolution according to time after Mn^{2+} injection in the ipsilateral internal capsule of vehicle KO AT and Epo D KO AT mice. (D) Histograms of slope averages for ipsi- and contralateral ROIs. (E) Histograms of the RSI averages for ipsi- and contralateral ROIs at 24 h after Mn^{2+} injection. n = 10 vehicle KO; n = 10 Epo D KO. The values are the mean ± SEM. *p < 0.05; **p < 0.01; ***p < 0.001. Abbreviations: Ant. TH: anterior thalamus; cp: cerebral peduncle; ic: internal capsule; Post. TH: posterior thalamus.

that were measured at 24 h were similar in all analyzed ROIs between the vehicle (DMSO KO BT) and the Epo D (Epo D KO BT) animals (Fig. 4B). After chronic treatment (AT) with Epo D (Epo D KO AT) or DMSO (vehicle KO AT), the distribution pattern of Mn^{2+} between both groups was qualitatively similar (data not shown).

The RSI values after treatment by either the Epo D or the vehicle were then measured. As illustrated in Fig. 4, panel C for the ipsilateral internal capsule (ic), RSI values increased linearly over time in both Epo D-treated mice (Epo D KO AT; $R^2 = 0.9709$, $p = 0.015$) and vehicle-treated mice (vehicle KO AT; $R^2 = 0.9654$; $p = 0.017$). However, strikingly, after chronic Epo D treatment, the slope value was higher by 67% ($p = 1.4 \times 10^{-4}$), which indicated that Epo D improved Mn^{2+} neuronal transport in KO mice rate in the ipsilateral internal capsule. Slope values were then calculated for each ROI, and the results clearly indicated that Epo D significantly increased the neuronal transport rate in almost all ipsi- and contralateral ROIs (Fig. 4D). In both ipsi- and contralateral ROIs, the slope value increased by an average of 51% ($p = 0.004$ and $p = 0.005$, respectively). These results showed that Epo D stimulated Mn^{2+} transport in an equivalent manner in both ipsi- and contralateral brain regions. To note, slope values of Epo D-treated KO mice (Fig. 4C; $y = 1.63$) did not reach that of WT mice (Fig. 2B; $y = 1.81$). The quantification of RSI intensities in all ROIs was then performed (Fig. 4E) and led to the same conclusions. In all ROIs at 24 h post-injection, RSI values of Epo D-treated mice were higher than values for vehicle-treated mice (Fig. 4E), with a similar increase of approximately 18% and 16% in ipsi- and contralateral ROIs, respectively ($p = 0.006$ and $p = 0.001$, respectively).

Altogether, these results showed that Epo D treatment strongly stimulates the neuronal transport of Mn^{2+}.

Discussion

In this study, using MEMRI in live animals, we showed that MAP6 KO mice exhibit an altered neuronal transport capacity, which is associated with a deficit in some white matter tracts. MAP6 KO mice transported less Mn^{2+} between the S1 cortex and projection areas than the WT control mice, particularly in contralateral structures. Mn^{2+} transport relies on axonal transport and on synaptic activity, which includes neurotransmitter liberation and re-uptake. The transport of Mn^{2+} is mediated by several mechanisms, which include the transport of intracellular vesicles (Pautler, 2004) and mitochondria (Morello et al., 2008), the stability of microtubules (Takeda et al., 1998), the viscosity of the cytosol, the efficiency of microtubule motors (Bearer et al., 2007), the intensity of the release and capture of synaptic vesicles (Drapeau and Nachshen, 1984; Pastor et al., 2008) and the number of axons. The abnormal neuronal transport that was observed in MAP6 mice can be the result of several abnormalities, such as reduced axonal tract size, reduced microtubule stability and abnormal synaptic efficiency. Indeed, we reported reductions in several tract sizes, which were associated with a reduction in the thalamic regions in MAP6 KO mice. These reductions might affect both the speed of neuronal transport (relative to the slope of RSI over time) and Mn^{2+} accumulation (relative to the RSI at 24 h post-injection). However, the reductions in axonal tracts do not fully contribute to this defect because the tract reduction is similar in both hemispheres, whereas the transport reduction is more severe in the contralateral region. In MAP6 KO brains, a reduced number of glutamatergic synaptic vesicles have been reported (Andrieux et al., 2002). This abnormality most likely is a crucial contributor to the neuronal transport deficit in the contralateral region, where synaptic transmission was required. Altogether, our results demonstrate that MEMRI was sensitive enough to characterize, *in vivo*, alterations of neuronal transport in MAP6 KO mice. Similar abnormal Mn^{2+} neuronal transport, as measured by MEMRI, has been reported for other animal models of psychiatric disorders and of neurodegenerative diseases, including Alzheimer's-related mutant mice (Bearer et al., 2007, 2009; Bertrand et al., 2013; Gallagher et al., 2012; Jouroukhin et al., 2013; Kim et al., 2011; Lutkenhoff et al., 2012; Sharp and Ross, 2012; Smith et al., 2007, 2010, 2011; Wang et al., 2012; Yu et al., 2011).

Epo D is a microtubule-stabilizing agent, which is related to taxol, but that has good blood–brain barrier permeability; when intraperitoneally injected, Epo D is retained in the brain (Brunden et al., 2010). The chronic treatment of MAP6 KO mice with a low dose Epo D has been shown to improve their cognitive behaviors and has been correlated with positive effects on synaptic vesicle number and synaptic plasticity within the hippocampus (Andrieux et al., 2006; Fournet et al., 2012). Here, we demonstrate that Epo D treatment strongly stimulates, in the same range, the speed of neuronal transport in both ipsi- and contralateral hemisphere sides. This improvement in neuronal transport might also contribute to the positive action of Epo D on integrated functions of MAP6 KO mice. The improvement of neuronal transport by Epo D might involve the amelioration of axonal transport. Indeed, in tauopathy models where the axonal transport is affected, a positive effect of Epo D treatment has been reported (Barten et al., 2012; Brunden et al., 2010; Zhang et al., 2012). At the molecular level, Epo D can affect microtubule dynamics by modifying microtubule stability, thereby regulating microtubule motor efficiency, which is known to be involved in the fast axonal transport of Mn^{2+}. Indeed, the molecular motors of the kinesin family are crucially involved in the fast axonal transport of Mn^{2+}; a kinesin light chain 1 KO mouse exhibited an alteration in neuronal transport, as assayed by MEMRI (Bearer et al., 2007). Epo D treatment might also modify microtubule density and reduce axonal dystrophy, as reported in the tauopathy mouse model (Zhang et al., 2012). These effects will directly improve fast axonal transport. In our study, Epo D treatment directly and strongly not only stimulates axonal transport, as witnessed by the increase in the slope of transported Mn^{2+} within ipsilateral monosynaptic tracts, but also seems to improve synaptic transmission because the speed of Mn^{2+} transport is also enhanced in polysynaptic contralateral tracts. Also, the comparison of slope values between WT mice and Epo D treated KO mice suggests partial recovery which might result from the axonal fiber loss observed in KO mice. The advantage of MEMRI is to provide an integrated view of all of the effects that occur at a molecular and a cellular level.

Notably, using MEMRI, another microtubule modulator, NAP (davunetide), has recently been shown to rescue neuronal transport defects in an amyotrophic lateral sclerosis animal model (Jouroukhin et al., 2013). Interestingly, NAP treatment has been reported to alleviate MAP6 cognitive disorders (Merenlender-Wagner et al., 2010). One might speculate that davunetide alleviation of MAP6 KO behavioral disorders can involve the amelioration of the neuronal transport deficit that we identified in this study.

Conclusions

In this study, using MEMRI in live animals, we showed that the MAP6 KO mouse, which is an animal model that is pertinent for the study of schizophrenia, exhibits an altered neuronal transport capacity, which is associated with a deficit in some white matter tracts. We demonstrated that Epo D is able to alleviate the neuronal transport defects that are exhibited by MAP6 KO mice and most likely contributes to the reported alleviation of behavioral and cognitive disorders (Andrieux et al., 2006; Fournet et al., 2012). Thus, complementary to molecular and cellular studies of neuronal transport, MEMRI is a power tool that can be used to reveal, *in vivo*, a neuronal transport deficit and to directly assay the positive impact of a pharmacological agent on this deficit.

Supplementary data to this article can be found online at http://dx.doi.org/10.1016/j.neuroimage.2014.03.071.

Acknowledgments

The authors acknowledge the excellent technical support of the MRI Facility of Grenoble (IRMaGe) and the company Helmholtz Zentrum für Infektionsforschung GmbH (Inhoffenstrasse 7, 38124 Braunschweig,

Germany) for providing Epothilone D. We thank E. Billet-Hernandez and O. Sarrault for animal care, V. Coizet for stereotaxic expertise and advice, J. Brocard for statistical advices and C. Delphin for critical reading of the manuscript. Part of this work was supported by the French National Research Agency (2010-BLAN-1202-01) Awards 2010 Blanc 120201 CBioS (to A.A.). A.D. received a stipend from the Région Rhône-Alpes — Cluster HVN.

References

Andrieux, A., Salin, P.A., Vernet, M., Kujala, P., Baratier, J., Gory-Fauré, S., Bosc, C., Pointu, H., Proietto, D., Schweitzer, A., Denarier, E., Klumperman, J., Job, D., 2002. The suppression of brain cold-stable microtubules in mice induces synaptic defects associated with neuroleptic-sensitive behavioral disorders. Genes Dev. 16, 2350–2364.

Andrieux, A., Salin, P., Schweitzer, A., Begou, M., Pachoud, B., Brun, P., Gory-Faure, S., Kujala, P., Suaud-Chagny, M.F., Hofle, G., Job, D., 2006. Microtubule stabilizer ameliorates synaptic function and behavior in a mouse model for schizophrenia. Biol. Psychiatry 60, 1224–1230.

Barten, D.M., Fanara, P., Andorfer, C., Hoque, N., Wong, P.Y., Husted, K.H., Cadelina, G.W., Decarr, L.B., Yang, L., Liu, V., Fessler, C., Protassio, J., Riff, T., Turner, H., Janus, C.G., Sankaranarayanan, S., Polson, C., Meredith, J.E., Gray, G., Hanna, A., Olson, R.E., Kim, S.H., Vite, G.D., Lee, F.Y., Albright, C.F., 2012. Hyperdynamic microtubules, cognitive deficits, and pathology are improved in tau transgenic mice with low doses of the microtubule-stabilizing agent BMS-241027. J. Neurosci. 32, 7137–7145.

Bearer, E.L., Falzone, T.L., Zhang, X., Biris, O., Rasin, A., Jacobs, R.E., 2007. Role of neuronal activity and kinesin on tract tracing by manganese-enhanced MRI (MEMRI). NeuroImage 37 (Suppl. 1), S37–S46.

Bearer, E.L., Zhang, X., Janvelyan, D., Boulat, B., Jacobs, R.E., 2009. Reward circuitry is perturbed in the absence of the serotonin transporter. NeuroImage 46, 1091–1104.

Bégou, M., Volle, J., Bertrand, J.B., Brun, P., Job, D., Schweitzer, A., Saoud, M., D'Amato, T., Andrieux, A., Suaud-Chagny, M.F., 2008. The stop null mice model for schizophrenia displays cognitive and social deficits partly alleviated by neuroleptics. Neuroscience 157, 29–39.

Bertrand, A., Khan, U., Hoang, D.M., Novikov, D.S., Krishnamurthy, P., Rajamohamed Sait, H.B., Little, B.W., Sigurdsson, E.M., Wadghiri, Y.Z., 2013. Non-invasive, in vivo monitoring of neuronal transport impairment in a mouse model of tauopathy using MEMRI. NeuroImage 64, 693–702.

Bouvrais-Veret, C., Weiss, S., Andrieux, A., Schweitzer, A., McIntosh, J.M., Job, D., Giros, B., Martres, M.P., 2007. Sustained increase of alpha7 nicotinic receptors and choline-induced improvement of learning deficit in STOP knock-out mice. Neuropharmacology 52, 1691–1700.

Brenner, E., Sonnewald, U., Schweitzer, A., Andrieux, A., Nehlig, A., 2007. Hypoglutamatergic activity in the STOP knockout mouse: a potential model for chronic untreated schizophrenia. J. Neurosci. Res. 85, 3487–3493.

Brun, P., Begou, M., Andrieux, A., Mouly-Badina, L., Clerget, M., Schweitzer, A., Scarna, H., Renaud, B., Job, D., Suaud-Chagny, M.F., 2005. Dopaminergic transmission in STOP null mice. J. Neurochem. 94, 63–73.

Brunden, K.R., Zhang, B., Carroll, J., Yao, Y., Potuzak, J.S., Hogan, A.M., Iba, M., James, M.J., Xie, S.X., Ballatore, C., Smith III, A.B., Lee, V.M., Trojanowski, J.Q., 2010. Epothilone D improves microtubule density, axonal integrity, and cognition in a transgenic mouse model of tauopathy. J. Neurosci. 30, 13861–13866.

Costas, J., Suarez-Rama, J.J., Carrera, N., Paz, E., Paramo, M., Agra, S., Brenlla, J., Ramos-Rios, R., Arrojo, M., 2013. Role of DISC1 interacting proteins in schizophrenia risk from genome-wide analysis of missense SNPs. Ann. Hum. Genet. 77, 504–512.

De Vos, K.J., Chapman, A.L., Tennant, M.E., Manser, C., Tudor, E.L., Lau, K.F., Brownlees, J., Ackerley, S., Shaw, P.J., McLoughlin, D.M., Shaw, C.E., Leigh, P.N., Miller, C.C., Grierson, A.J., 2007. Familial amyotrophic lateral sclerosis-linked SOD1 mutants perturb fast axonal transport to reduce axonal mitochondria content. Hum. Mol. Genet. 16, 2720–2728.

Delotterie, D., Ruiz, G., Brocard, J., Schweitzer, A., Roucard, C., Roche, Y., Suaud-Chagny, M.F., Bressand, K., Andrieux, A., 2010. Chronic administration of atypical antipsychotics improves behavioral and synaptic defects of STOP null mice. Psychopharmacology (Berl.) 208, 131–141.

Drapeau, P., Nachshen, D.A., 1984. Manganese fluxes and manganese-dependent neurotransmitter release in presynaptic nerve endings isolated from rat brain. J. Physiol. 348, 493–510.

Fitzsimmons, J., Kubicki, M., Smith, K., Bushell, G., Estepar, R.S., Westin, C.F., Nestor, P.G., Niznikiewicz, M.A., Kikinis, R., McCarley, R.W., Shenton, M.E., 2009. Diffusion tractography of the fornix in schizophrenia. Schizophr. Res. 107, 39–46.

Fournet, V., Jany, M., Fabre, V., Chali, F., Orsal, D., Schweitzer, A., Andrieux, A., Messanvi, F., Giros, B., Hamon, M., Lanfumey, L., Deloulme, J.C., Martres, M.P., 2010. The deletion of the microtubule-associated STOP protein affects the serotonergic mouse brain network. J. Neurochem. 115, 1579–1594.

Fournet, V., de Lavilleon, G., Schweitzer, A., Giros, B., Andrieux, A., Martres, M.P., 2012. Both chronic treatments by epothilone D and fluoxetine increase the short-term memory and differentially alter the mood-status of STOP/MAP6 KO mice. J. Neurochem. 123, 982–996.

Fradley, R.L., O'Meara, G.F., Newman, R.J., Andrieux, A., Job, D., Reynolds, D.S., 2005. STOP knockout and NMDA NR1 hypomorphic mice exhibit deficits in sensorimotor gating. Behav. Brain Res. 163, 257–264.

Friocourt, G., Marcorelles, P., Saugier-Veber, P., Quille, M.L., Marret, S., Laquerriere, A., 2011. Role of cytoskeletal abnormalities in the neuropathology and pathophysiology of type I lissencephaly. Acta Neuropathol. 121, 149–170.

Gallagher, J.J., Zhang, X., Ziomek, G.J., Jacobs, R.E., Bearer, E.L., 2012. Deficits in axonal transport in hippocampal-based circuitry and the visual pathway in APP knock-out animals witnessed by manganese enhanced MRI. NeuroImage 60, 1856–1866.

Jouroukhin, Y., Ostritsky, R., Assaf, Y., Pelled, G., Giladi, E., Gozes, I., 2013. NAP (davunetide) modifies disease progression in a mouse model of severe neurodegeneration: protection against impairments in axonal transport. Neurobiol. Dis. 56, 79–94.

Kim, J., Choi, I.Y., Michaelis, M.L., Lee, P., 2011. Quantitative in vivo measurement of early axonal transport deficits in a triple transgenic mouse model of Alzheimer's disease using manganese-enhanced MRI. NeuroImage 56, 1286–1292.

Leergaard, T.B., Bjaalie, J.G., Devor, A., Wald, L.L., Dale, A.M., 2003. In vivo tracing of major rat brain pathways using manganese-enhanced magnetic resonance imaging and three-dimensional digital atlasing. NeuroImage 20, 1591–1600.

Lutkenhoff, E., Karlsgodt, K.H., Gutman, B., Stein, J.L., Thompson, P.M., Cannon, T.D., Jentsch, J.D., 2012. Structural and functional neuroimaging phenotypes in dysbindin mutant mice. NeuroImage 62, 120–129.

Merenlender-Wagner, A., Pikman, R., Giladi, E., Andrieux, A., Gozes, I., 2010. NAP (davunetide) enhances cognitive behavior in the STOP heterozygous mouse—a microtubule-deficient model of schizophrenia. Peptides 31, 1368–1373.

Morello, M., Canini, A., Mattioli, P., Sorge, R.P., Alimonti, A., Bocca, B., Forte, G., Martorana, A., Bernardi, G., Sancesario, G., 2008. Sub-cellular localization of manganese in the basal ganglia of normal and manganese-treated rats: an electron spectroscopy imaging and electron energy-loss spectroscopy study. Neurotoxicology 29, 60–72.

Narita, K., Kawasaki, F., Kita, H., 1990. Mn and Mg influxes through Ca channels of motor nerve terminals are prevented by verapamil in frogs. Brain Res. 510, 289–295.

Palau-Baduell, M., Salvadó-Salvadó, B., Clofent-Torrentó, M., Valls-Santasusana, A., 2012. Autism and neural connectivity. Rev. Neurol. 54 (Suppl. 1), S31–S39.

Pastor, M.T., Kummerer, N., Schubert, V., Esteras-Chopo, A., Dotti, C.G., Lopez de la Paz, M., Serrano, L., 2008. Amyloid toxicity is independent of polypeptide sequence, length and chirality. J. Mol. Biol. 375, 695–707.

Patterson, J.V., Hetrick, W.P., Boutros, N.N., Jin, Y., Sandman, C., Stern, H., Potkin, S., Bunney Jr., W.E., 2008. P50 sensory gating ratios in schizophrenics and controls: a review and data analysis. Psychiatry Res. 158, 226–247.

Pautler, R.G., 2004. In vivo, trans-synaptic tract-tracing utilizing manganese-enhanced magnetic resonance imaging (MEMRI). NMR Biomed. 17, 595–601.

Pautler, R.G., Koretsky, A.P., 2002. Tracing odor-induced activation in the olfactory bulbs of mice using manganese-enhanced magnetic resonance imaging. NeuroImage 16, 441–448.

Pautler, R.G., Silva, A.C., Koretsky, A.P., 1998. In vivo neuronal tract tracing using manganese-enhanced magnetic resonance imaging. Magn. Reson. Med. 40, 740–748.

Paxinos, G., Watson, C., 1998. The Rat Brain in Sterotaxic Coordinates. Academic Press, San Diego.

Powell, K.J., Hori, S.E., Leslie, R., Andrieux, A., Schellinck, H., Thorne, M., Robertson, G.S., 2007. Cognitive impairments in the STOP null mouse model of schizophrenia. Behav. Neurosci. 121, 826–835.

Raponi, E., Agenes, F., Delphin, C., Assard, N., Baudier, J., Legraverend, C., Deloulme, J.C., 2007. S100B expression defines a state in which GFAP-expressing cells lose their neural stem cell potential and acquire a more mature developmental stage. Glia 55, 165–177.

Saleem, K.S., Pauls, J.M., Augath, M., Trinath, T., Prause, B.A., Hashikawa, T., Logothetis, N.K., 2002. Magnetic resonance imaging of neuronal connections in the macaque monkey. Neuron 34, 685–700.

Schmued, L., Bowyer, J., Cozart, M., Heard, D., Binienda, Z., Paule, M., 2008. Introducing Black-Gold II, a highly soluble gold phosphate complex with several unique advantages for the histochemical localization of myelin. Brain Res. 1229, 210–217.

Sharp, D.J., Ross, J.L., 2012. Microtubule-severing enzymes at the cutting edge. J. Cell Sci. 125, 2561–2569.

Smith, K.D., Kallhoff, V., Zheng, H., Pautler, R.G., 2007. In vivo axonal transport rates decrease in a mouse model of Alzheimer's disease. NeuroImage 35, 1401–1408.

Smith, K.D., Peethumnongsin, E., Lin, H., Zheng, H., Pautler, R.G., 2010. Increased human wildtype tau attenuates axonal transport deficits caused by loss of APP in mouse models. Magn. Reson. Insights 4, 11–18.

Smith, K.D., Paylor, R., Pautler, R.G., 2011. R-flurbiprofen improves axonal transport in the Tg2576 mouse model of Alzheimer's disease as determined by MEMRI. Magn. Reson. Med. 65, 1423–1429.

Soria, G., Wiedermann, D., Justicia, C., Ramos-Cabrer, P., Hoehn, M., 2008. Reproducible imaging of rat corticothalamic pathway by longitudinal manganese-enhanced MRI (L-MEMRI). NeuroImage 41, 668–674.

Stokin, G.B., Lillo, C., Falzone, T.L., Brusch, R.G., Rockenstein, E., Mount, S.L., Raman, R., Davies, P., Masliah, E., Williams, D.S., Goldstein, L.S., 2005. Axonopathy and transport deficits early in the pathogenesis of Alzheimer's disease. Science 307, 1282–1288.

Szebenyi, G., Morfini, G.A., Babcock, A., Gould, M., Selkoe, K., Stenoien, D.L., Young, M., Faber, P.W., MacDonald, M.E., McPhaul, M.J., Brady, S.T., 2003. Neuropathogenic forms of huntingtin and androgen receptor inhibit fast axonal transport. Neuron 40, 41–52.

Takeda, A., Kodama, Y., Ishiwatari, S., Okada, S., 1998. Manganese transport in the neural circuit of rat CNS. Brain Res. Bull. 45, 149–152.

Taya, S., Shinoda, T., Tsuboi, D., Asaki, J., Nagai, K., Hikita, T., Kuroda, S., Kuroda, K., Shimizu, M., Hirotsune, S., Iwamatsu, A., Kaibuchi, K., 2007. DISC1 regulates the transport of the NUDEL/LIS1/14-3-3epsilon complex through kinesin-1. J. Neurosci. 27, 15–26.

Tucciarone, J., Chuang, K.H., Dodd, S.J., Silva, A., Pelled, G., Koretsky, A.P., 2009. Layer specific tracing of corticocortical and thalamocortical connectivity in the rodent using manganese enhanced MRI. NeuroImage 44, 923–931.

Van der Linden, A., Verhoye, M., Van Meir, V., Tindemans, I., Eens, M., Absil, P., Balthazart, J., 2002. In vivo manganese-enhanced magnetic resonance imaging reveals connections and functional properties of the songbird vocal control system. Neuroscience 112, 467–474.

Volle, J., Brocard, J., Saoud, M., Gory-Faure, S., Brunelin, J., Andrieux, A., Suaud-Chagny, M.F., 2013. Reduced expression of STOP/MAP6 in mice leads to cognitive deficits. Schizophr. Bull. 39, 969–978.

von Bartheld, C.S., Cunningham, D.E., Rubel, E.W., 1990. Neuronal tracing with DiI: decalcification, cryosectioning, and photoconversion for light and electron microscopic analysis. J. Histochem. Cytochem. 38, 725–733.

Wang, F.H., Appelkvist, P., Klason, T., Gissberg, O., Bogstedt, A., Eliason, K., Martinsson, S., Briem, S., Andersson, A., Visser, S.A., Ivarsson, M., Lindberg, M., Agerman, K., Sandin, J., 2012. Decreased axonal transport rates in the Tg2576 APP transgenic mouse: improvement with the gamma-secretase inhibitor MRK-560 as detected by manganese-enhanced MRI. Eur. J. Neurosci. 36, 3165–3172.

Willemsen, M.H., Vissers, L.E., Willemsen, M.A., van Bon, B.W., Kroes, T., de Ligt, J., de Vries, B.B., Schoots, J., Lugtenberg, D., Hamel, B.C., van Bokhoven, H., Brunner, H.G., Veltman, J.A., Kleefstra, T., 2012. Mutations in DYNC1H1 cause severe intellectual disability with neuronal migration defects. J. Med. Genet. 49, 179–183.

Yu, X., Wadghiri, Y.Z., Sanes, D.H., Turnbull, D.H., 2005. In vivo auditory brain mapping in mice with Mn-enhanced MRI. Nat. Neurosci. 8, 961–968.

Yu, X., Nieman, B.J., Sudarov, A., Szulc, K.U., Abdollahian, D.J., Bhatia, N., Lalwani, A.K., Joyner, A.L., Turnbull, D.H., 2011. Morphological and functional midbrain phenotypes in Fibroblast Growth Factor 17 mutant mice detected by Mn-enhanced MRI. NeuroImage 56, 1251–1258.

Zhang, B., Carroll, J., Trojanowski, J.Q., Yao, Y., Iba, M., Potuzak, J.S., Hogan, A.M., Xie, S.X., Ballatore, C., Smith III, A.B., Lee, V.M., Brunden, K.R., 2012. The microtubule-stabilizing agent, epothilone D, reduces axonal dysfunction, neurotoxicity, cognitive deficits, and Alzheimer-like pathology in an interventional study with aged tau transgenic mice. J. Neurosci. 32, 3601–3611.